Supporting Information

Hainmüller et al. 10.1073/pnas.1409394111

SI Materials and Methods

Immunohistochemistry. ***Tissue preparation.*** Wistar rats [postnatal day (P) 20–P23] were deeply anesthetized by brief exposure to isoflurane and subsequent i.p. injection of urethane (2 g/kg in 0.1 M PBS). Depth of anesthesia was judged by testing pinch-withdrawal and corneal reflexes. Surgery was only commenced after their cessation. Hearts of the animals were exposed surgically, a canula was inserted into the aorta, and the right atrium was incised. Animals were briefly perfused with 0.1 M PBS (1–2 min) and subsequently for 13 min with fixatives for light microscopy [0.1 M PBS with 4% (vol/vol) paraformaldehyde (PFA)] or EM [0.1 M PBS with 4% (vol/vol) PFA, 15% (vol/vol) picric acid, and 0.05% glutaraldehyde]. After fixation, brains were removed and washed in 0.1 M PBS.

Antibodies. All antibodies used in this study are commercially available and have been tested for specificity on tissue of KO animals (1–3). Parvalbumin (PV)-expressing neurons were identified with a rabbit (RB) polyclonal antibody (SWANT) diluted 1:1,000 for immunofluorescence and immunoperoxidase reactions and 1:200 for immunogold labeling. For detection of metatropic glutamate receptor 1α (mGluR1α), an affinity-purified, polyclonal antibody raised in guinea pig (GP) (Frontier Institute) was used diluted to 1 μg/mL for immunofluorescence, 2 μg/mL for peroxidase reaction, and 2.9 μg/mL for immunogold labeling. MGluR5 was detected with an affinity-purified, polyclonal GP antibody (Frontier Institute) used at dilutions of 1 μg/mL for immunofluorescence, 2 μg/mL for peroxidase reaction, and 4 μg/mL for immunogold labeling. We used secondary antibodies against RB coupled to Cy3 (1:1,000; Invitrogen) and against GP coupled to Alexa Fluor 647 (1:1,000; Invitrogen) to visualize immunolabeling for fluorescence microscopy. Biotinylated antibodies against GP or RB (Vector Laboratories) were diluted at a ratio of 1:50, and 1.4 nm of gold-coupled secondary antibodies (Nanogold; Nanoprobes) was diluted at a ratio of 1:100.

Immunofluorescence microscopy. For fluorescence microscopy, blocks of brain containing the hippocampal formation were trimmed and cut into 50-μm thick sections with a vibratome (DTK-1000; Dosaka). After cutting, slices were washed in 0.1 M PBS and then permeabilized with PBS containing 0.4% Triton X-100 for 30 min. Afterward, nonspecific binding sites in the sections were blocked with PBS containing 4% (vol/vol) normal goat serum (NGS) and 0.2% Triton X-100. Sections were then incubated overnight at 4 °C with a mixture of primary antibodies against PV and mGluR1α or mGluR5 prepared in PBS with 0.1% Triton X-100 and 2% (vol/vol) NGS. On the next day, sections were washed two times in PBS plus 1% NGS and then incubated in PBS plus 1.5% (vol/vol) NGS and Cy3-conjugated goat–anti-RB plus Alexa Fluor 647-conjugated goat–anti-GP secondary antibodies for 2–3 h at room temperature (22 °C). Sections were washed again in PBS afterward and mounted in Mowiol (Carl Roth GmbH). Confocal fluorescence images and image stacks from the sections were obtained using an LSM 710 confocal scanning microscope (Zeiss) with a 63× objective (N.A. of 1.4).

Preembedding immunoelectron microscopy. To prepare samples for EM with preembedding immunohistochemistry, brains were first transferred to a cryoprotection solution made of 0.1 M PBS containing 10% (wt/vol) sucrose; after 2 h, they were transferred to PBS with 20% (wt/vol) sucrose, where the brains remained until they were equilibrated to the extent that they sank to the ground level of the solution (~12 h). Brains were quickly frozen over liquid nitrogen, thawed, and washed in 0.1 M phosphate buffer. Afterward, 50-μm thick sections were cut with a vibratome as described above for light microscopy. We performed double labeling against PV and mGluR1α, as well as against PV and mGluR5 (4). Sections were washed and blocked in a solution of 20% (vol/vol) NGS in Tris-buffered saline (TBS) for 1 h and afterward incubated with the primary antibodies in TBS plus 3% (vol/vol) NGS overnight at 4 °C. On the next day, sections were washed in TBS and subsequently incubated for 2 h at room temperature with biotinylated- or 1.4-nm gold-coupled secondary antibodies (Nanogold) in TBS plus 2% (vol/vol) NGS. Sections were then washed and postfixated with 1% glutaraldehyde in 25 mM PBS for 10 min. Gold labeling in the sections was then intensified using an HQ-Silver kit (Nanoprobes) for 8–12 min. Afterward, sections were washed and incubated with the avidin-biotin peroxidase complex (ABC Kit; Vector Laboratories), and peroxidase was visualized with 3,3′-diaminobenzidine tetrahydrochloride (0.05%) as a chromogen and 0.01% H_2O_2 as a substrate. Finally, sections were treated with OsO_4, stained with uranyl acetate, dehydrated, and flat-embedded in Durcupan resin (Fluka). Small (~0.3 mm × 0.3 mm) blocks of the dentate gyrus (DG) hilar region were excised from the flat-embedded sections and reembedded in resin. Ultrathin (60–80 nm) sections were then cut from the immediate surface of the blocks with an ultramicrotome (EM UC7; Leica) and inspected in a transmission electron microscope (Leo 906E; Zeiss). For 3D reconstructions, a series of 10–42 adjacent sections was collected, and individual dendritic profiles were acquired subsequently in each section (5).

Three-dimensional reconstructions from ultrathin sections. Serial sections were aligned and reconstructed using the free software Reconstruct (courtesy of K. M. Harris, University of Texas, Austin, TX) (6). Postsynaptic densities (PSDs) of asymmetrical synapses were detected and reconstructed throughout the series. Gold particles detected within a 35-nm radius from the outer dendritic membrane were considered as specific labeling of membrane-associated proteins (7) and were marked in the reconstructed 3D space, and the distance to the closest PSD was determined. In this way, we localized a total of 450 particles labeling mGluR5 proteins and 202 PSDs within seven dendritic segments. Finally, the distribution of distances was grouped into 60-nm bins, starting from the PSD edge to obtain a histogram of the distribution of extrasynaptic receptors. To assess the density and specificity of immunogold labeling, we calculated the density of gold particles in an area within 35 nm inside the membrane border and compared it with the density measured over mitochondria in the same sections. Membrane-bound labeling for mGluR5 (12.44 ± 2.89 particles per square micrometer) was significantly higher than labeling over mitochondria (0.4 ± 0.08 particles per square micrometer) in all reconstructed dendrites (seven dendrites, $P \leq 0.031$ for all samples).

Electrophysiology. ***Acute hippocampal slice preparation.*** Transverse 300-μm thick hippocampal slices were cut from Wistar rats (P17–P23) with a vibratome (VT1200; Leica) as described earlier (8). After cutting, slices were stored in artificial cerebrospinal fluid (ACSF) containing the following: 125 mM NaCl, 25 mM $NaHCO_3$, 2.5 mM KCl, 1.25 mM NaH_2PO_4, 25 mM glucose, 2 mM $CaCl_2$, and 1 mM $MgCl_2$. The same solution was used for superfusion during the recordings. ACSF was equilibrated with a 95% O_2 and 5% CO_2 gas mixture throughout experiments.

Single and dual whole-cell patch-clamp recordings. Patch pipettes for whole-cell patch-clamp recordings were pulled from borosilicate glass capillaries (2-mm o.d. and 0.5-mm wall thickness) with a micropipette puller (P-97; Sutter Instruments). Pipettes with tip resistances ranging from 2–4 MΩ were used for recordings from

perisomatic inhibitory interneurons (PIIs), and pipettes with tip resistances ranging from 3–5 MΩ were used for recordings from granule cells (GCs). Pipettes were filled with an internal solution containing the following: 120 mM K-gluconate, 20 mM KCl, 0.1 mM EGTA, 2 mM $MgCl_2$, 4 mM Na_2-ATP, 0.5 mM GTP, 10 mM Hepes, 7 mM Na_2-phosphocreatine, and 0.2% biocytin, with a pH of 7.2 and an osmolarity of ∼300 mOsm. In a subset of experiments (four PIIs), 0.1 mM spermine was added to the pipette solution. Stimulus electrodes for extracellular mossy fiber (MF) stimulation were made of glass capillaries filled with a sodium-rich, Hepes-buffered solution containing the following: 135 mM NaCl, 5.4 mM KCl, 1.8 mM $CaCl_2$, 1 mM $MgCl_2$, and 5 mM Hepes. All chemicals were obtained from Sigma–Aldrich and Tocris. Recordings were performed in a submerged recording chamber superfused with carbogenated ACSF at near-physiological temperatures (30–34 °C).

Slices were visualized with infrared-differential interference contrast microscopy (9), and putative PIIs were identified by their localization in the GC layer or at the border between the GC layer and the hilus and their large multipolar somata. After whole-cell recordings were established, PIIs were further identified by the frequent occurrence of spontaneous excitatory postsynaptic currents (EPSCs) with fast kinetics (10), low-input resistance (<100 MΩ), and the generation of high-frequency (>100 Hz) action potentials (APs) in response to step current injections (1 nA for 1 s) in the current-clamp configuration.

For paired GC-PII recordings, GCs at the border of the molecular layer were selected. After whole-cell recording had been established from a GC, single APs were evoked by brief (1–2 ms) current injections, and unitary EPSCs in the PII were measured at a holding potential of −70 mV. Experiments with extracellular MF stimulation were performed as previously described (8). MF-mediated EPSCs were identified by their characteristic rapid time course and paired-pulse facilitation (10). In a subset of recordings, their identity was confirmed by their sensitivity to bath application of (2S,2′R,3′R)-2-(2′,3′-Dicarboxycyclopropyl)glycine (DCG-IV; 0.5 μM; main text). $GABA_A$ receptor-mediated inhibitory postsynaptic currents (11) were blocked by bath application of the $GABA_A$ receptor antagonist SR 95531 (5 μM) throughout all experiments involving extracellular stimulation. Pharmacological agents were bath-applied 5–10 min before application of plasticity protocols. To deplete internal Ca^{2+} stores, we preincubated slices for 30–60 min in cyclopiazonic acid (CPA; 30 μM). CPA was also present in the bath during recordings. Similarly, intracellular agents (GDP-β-s, PKC 19-36) were dialyzed via the patch pipette for at least 30 min before the start of the measurements. Series resistance (R_s) was monitored but not compensated, and recordings were discarded if the R_s in the recorded PII changed by more than 20%. The effect of bath-applied (S)-3,5-dihydroxyphenylglycine (DHPG; 100 μM) on synaptic transmission at paired GC-PII recordings was observed by monitoring the PII holding current (Fig. S3*E*). Nimodipine (10 μM) and Ni^{2+} (50 μM) were added to the bath for blocking voltage-dependent Ca^{2+} channels (VDCCs). Nimodipine solutions were prepared every day freshly from frozen stock aliquots, and great care was taken to keep all solutions in absolute darkness because dihydropyridines are highly light-sensitive.

One Multiclamp 700B or two Axopatch 200B amplifiers (Molecular Devices) were used for single-cell and paired whole-cell recordings. Data were filtered at 10 kHz and acquired at 20 kHz (voltage-clamp recordings) or 50 kHz (current-clamp recordings) with a CED 1401 interface (Cambridge Instruments) and custom-written software (FPulse; courtesy of U. Fröbe, Institute for Physiology I, University of Freiburg). Data analysis was performed using StimFit (courtesy of C. Schmidt-Hieber, University College London, London) and custom-made scripts in Python.

Visualization and immunohistochemical identification of recorded cells. Cells were filled during recordings with 0.1–0.2% biocytin. Slices were fixed with 0.1 M PBS containing 4% (vol/vol) PFA. Biocytin-filled neurons were visualized with Alexa Fluor 647-conjugated avidin. Neurons were morphologically identified with either a LSM 710 confocal microscope (Zeiss) or an Axioskop 2FS (Zeiss) epifluorescence microscope. PIIs were identified on the basis of their extensive axonal arborization, which was largely located in the GC layer. GCs were identified by their spiny apical dendrites, a lack of hilar dendritic processes, and a sparse axon projecting through the hilus to the stratum lucidum of CA3. The molecular identity of PII was further confirmed by antibody labeling against PV in a subset of 27 recorded PIIs.

Ca^{2+} Imaging. ***One-photon excitation high-speed CCD Ca^{2+} imaging.*** For one-photon imaging, PIIs were filled via the patch pipette with a pipette solution containing the following: 120 mM K-gluconate, 20 mM KCl, 2 mM $MgCl_2$, 4 mM Na_2ATP, 0.5 mM GTP, 10 mM Hepes, 7 mM Na_2-phosphocreatine, and 0.2% biocytin (imaging solution) added to 100 μM Oregon Green 488 BAPTA-1 [1,2-bis(o-aminoethyl ether)-N,N,N′,N′-tetraacetic acid-1 488] (Invitrogen). Cells were dialyzed for 15–20 min before the onset of imaging to allow equilibration of the soma and proximal dendrites with the internal solution. Fluorescence signals were visualized using an upright microscope (Axio Examiner; Zeiss) and excited with a light-emitting diode illumination system (CoolLED). Fluorescence signals were acquired at 125 or 500 Hz with a high-speed CCD camera (Neuroccd; RedShirt Imaging). Signals were stored on a personal computer and analyzed using custom scripts (courtesy of C. Elgueta, University of Freiburg, Freiburg, Germany) written in Igor (WaveMetrics).

To elicit group I mGluR-mediated Ca^{2+} responses (12) in PIIs, a glass capillary filled with ACSF containing 100 μM of the group I mGluR agonist DHPG (Tocris) was placed close to a PII basal dendrite. Transistor–transistor logic-triggered, brief pressure-puff application (20–100 ms, 500–700 mbar) was exerted with a pressure pulse generator (Mikrospritzer, courtesy of U. Fröbe, University of Freiburg, Freiburg, Germany). DHPG puffs were applied at intervals of 3 min. Fluorescence signals were analyzed within a region of interest containing the PII soma and proximal dendrite. After three to four puff stimulations, pharmacological agents were applied to the bath (*Results*) and the remaining Ca^{2+} signal was quantified. DHPG-induced changes in green fluorescence (ΔF) were calculated relative to baseline (0.1 s before stimulation) and expressed as $\%\Delta F/F_0 = [(F - F_{rest})/F_{rest}] \times 100$. For comparison of fluorescence signals before and after drug application, the average $\%\Delta F/F_0$ integral measured >6 min after drug application was divided by the mean $\%\Delta F/F_0$ integral before drug application. Integrals of fluorescence signals were stable for time spans exceeding the duration of the experiments in the absence of drug application (Fig. S3*F*).

Two-photon excitation laser-scanning Ca^{2+} imaging. For two-photon imaging, neurons were loaded with the Ca^{2+}-insensitive dye Alexa Fluor 594 (100 μM; Invitrogen), and the low-affinity (K_d = 2.3 μM) Ca^{2+}-sensitive dye Fluo-5F (300 μM; Invitrogen) was added to the internal solution described above. In another subset of experiments, Fluo-4FF (Invitrogen; 0.5 mM) was added as a Ca^{2+} indicator (five PIIs). PIIs were loaded with dyes for 20–30 min during whole-cell recordings before the onset of the imaging to ensure equilibration of the Ca^{2+} indicators. Imaging was performed with a galvanometric laser-scanning microscope system (Femto 2D; Femtonics) through a 40× water immersion objective (0.8 N.A.; Zeiss) with a wavelength-tunable IR laser (Chameleon Ultra II; Coherent) at 800 nm, with an 80-MHz pulse rate and a 140-fs pulse-width. First, the dendritic morphology of the PII was visualized by raster scanning. Then, a stimulus electrode was placed in close vicinity (∼10 μm) to the dendrite of interest to stimulate local synaptic inputs. Fluorescence signals in response to

synaptic stimulation were detected with a longitudinal line scan following the dendritic trajectory (Fig. S3 *A* and *B*). Under these conditions, narrow and highly localized hotspots of strongly changing fluorescence signals were detected that rapidly declined in both sites along the dendrites (Fig. S3*D*). These hotspots were identified as extracellularly stimulated synaptic contacts (13). A short (2–5 μm) scan line diagonal to the dendritic main axis was placed through the middle of the identified hotspots for the experiments shown in Fig. 4*A*. We refer to these signals as putative MF-mediated Ca^{2+} transients.

Fluorescence signals were acquired for three different stimuli: (*i*) a burst of APs generated in the PII soma and back-propagating to the basal PII dendrite (AP protocol), activating VDCCs consisting of 25 APs at 30 Hz; (*ii*) extracellular burst stimulation of MFs consisting of 25 stimuli at 30 Hz (non-associative burst-frequency simulation); and (*iii*) an associative burst-frequency stimulation, in which MF stimulation was paired with postsynaptic AP generation with a delay of 2 ms (25 pairings at 30 Hz). The three stimulation protocols were repeated five to 12 times in a pseudorandom order. Next, pharmacological agents were bath-applied for 5 min, and the same protocols were repeated. The change in Ca^{2+} signals was quantified [peak of green fluorescence change (ΔG)] and normalized to the background-corrected mean red fluorescence (R_0) signal for each pixel (ΔG/R). The Ca^{2+} signals remaining after the pharmacological blockade were calculated as mean ΔG/R evoked by a given protocol and normalized to ΔG/R evoked by the same protocol before pharmacological blockade. Data were analyzed using custom-written scripts in MATLAB (MathWorks).

Statistical Analysis. Statistical tests were performed using SigmaPlot 11 (SyStat). All values are given as the mean ± SEM. Statistical differences in the means of two samples were assessed by a two-tailed unpaired or paired *t* test for independent and related sample sets, respectively, if the samples were normally distributed, as determined by the Shapiro–Wilk test. If the normality test failed, the nonparametric Mann–Whitney *U* test was used. Significance levels are indicated as *P* values.

1. Schwaller B, et al. (1999) Prolonged contraction-relaxation cycle of fast-twitch muscles in parvalbumin knockout mice. *Am J Physiol* 276(2 Pt 1):C395–C403.
2. Tanaka J, et al. (2000) Gq protein alpha subunits Galphaq and Galpha11 are localized at postsynaptic extra-junctional membrane of cerebellar Purkinje cells and hippocampal pyramidal cells. *Eur J Neurosci* 12(3):781–792.
3. Uchigashima M, et al. (2007) Subcellular arrangement of molecules for 2-arachidonoylglycerol-mediated retrograde signaling and its physiological contribution to synaptic modulation in the striatum. *J Neurosci* 27(14):3663–3676.
4. Kulik A, et al. (2003) Subcellular localization of metabotropic GABA(B) receptor subunits GABA(B1a/b) and GABA(B2) in the rat hippocampus. *J Neurosci* 23(35): 11026–11035.
5. Kulik A, et al. (2002) Distinct localization of GABA(B) receptors relative to synaptic sites in the rat cerebellum and ventrobasal thalamus. *Eur J Neurosci* 15(2):291–307.
6. Fiala J, Harris K (2002) Computer-based alignment and reconstruction of serial sections. Microscopy and analysis. *Microsc Anal (Am Ed)* 52:5–7.
7. Nakamura M, et al. (2004) Signaling complex formation of phospholipase Cbeta4 with metabotropic glutamate receptor type 1alpha and 1,4,5-trisphosphate receptor at the perisynapse and endoplasmic reticulum in the mouse brain. *Eur J Neurosci* 20(11): 2929–2944.
8. Sambandan S, Sauer J-F, Vida I, Bartos M (2010) Associative plasticity at excitatory synapses facilitates recruitment of fast-spiking interneurons in the dentate gyrus. *J Neurosci* 30(35):11826–11837.
9. Bartos M, Vida I, Frotscher M, Geiger JR, Jonas P (2001) Rapid signaling at inhibitory synapses in a dentate gyrus interneuron network. *J Neurosci* 21(8):2687–2698.
10. Geiger JR, Lübke J, Roth A, Frotscher M, Jonas P (1997) Submillisecond AMPA receptor-mediated signaling at a principal neuron-interneuron synapse. *Neuron* 18(6):1009–1023.
11. Bartos M, et al. (2002) Fast synaptic inhibition promotes synchronized gamma oscillations in hippocampal interneuron networks. *Proc Natl Acad Sci USA* 99(20): 13222–13227.
12. Topolnik L, Azzi M, Morin F, Kougioumoutzakis A, Lacaille J-C (2006) mGluR1/5 subtype-specific calcium signalling and induction of long-term potentiation in rat hippocampal oriens/alveus interneurones. *J Physiol* 575(Pt 1):115–131.
13. Goldberg JH, Tamas G, Aronov D, Yuste R (2003) Calcium microdomains in aspiny dendrites. *Neuron* 40(4):807–821.

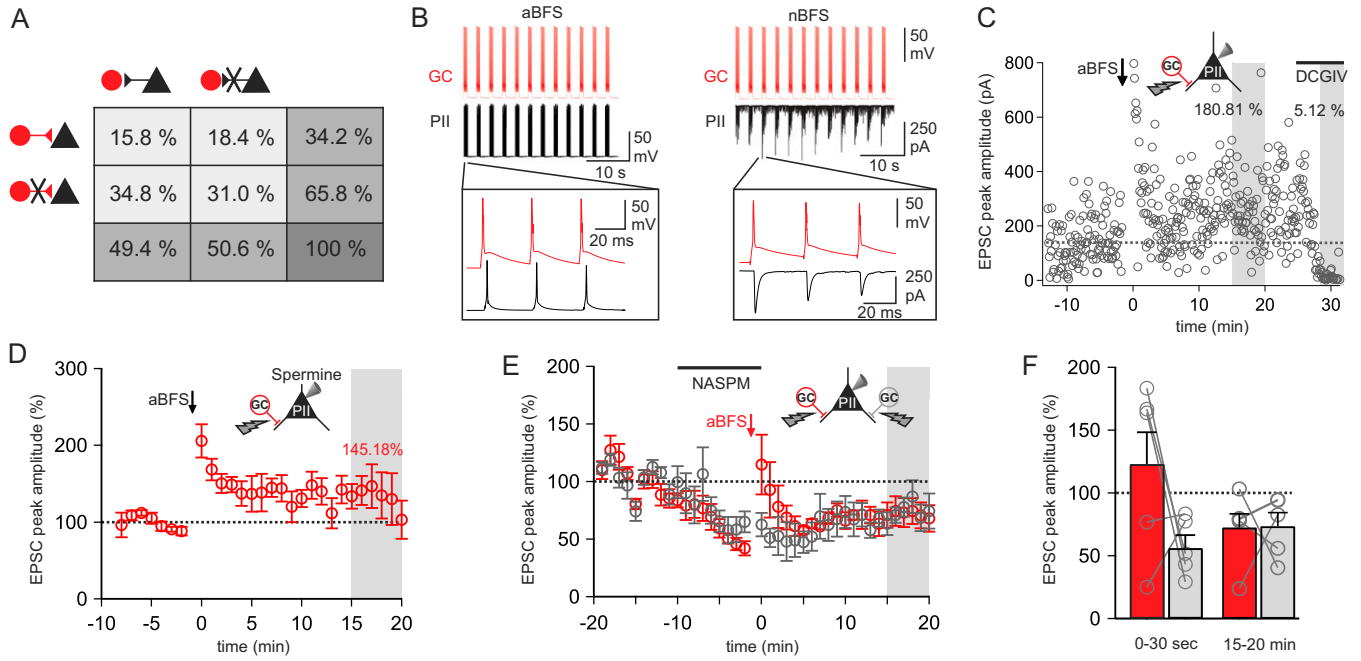

Fig. S1. Long-term plasticity at MF-PII synapses. (*A*) Table summarizes the connectivity between GCs and PIIs from the total number of simultaneous dual GC (red ●) and PII (black ▲) recordings. The first row contains the fraction of pairs that were mutually connected (excitatory and inhibitory synapses, first column) or unidirectionaly connected by excitatory synapses (second column). The first row of the third column represents the sum of the first and second columns, and thereby shows the total fraction of glutamatergic GC-PII pairs. The second row represents the group of pairs that were connected by inhibitory synapses (first column) or not connected (second column). (*B*) Illustration of the details of the associative burst-frequency stimulation (aBFS; *Left*) and the nonassociative burst-frequency stimulation (nBFS; *Right*) protocols. Bursts of single APs are shown (*Upper*; GC, red; PII, black), and the evoked unitary EPSCs (uEPSCs) recorded in a PII are depicted (*Lower Right*; black individual trace) during a GC-PII paired recording. The aBFS consisted of 25 APs evoked in the GC at a frequency of 30 Hz by brief current injection (2 ms, 1–2 nA). Bursts were repeated 12 times at 0.33 Hz. The PII was held in current-clamp configuration, and APs were elicited by brief current injection with a 1- to 3-ms delay. Thus, the onset of individual MF-mediated EPSCs preceded by 1–3 ms the somatically evoked PII APs. Similar to the aBFS, the nBFS consisted of 25 presynaptic APs at a frequency of 30 Hz that were repeated 12 times at 0.33 Hz. APs were elicited in the GC while the PII was held in voltage-clamp configuration at −70 mV. The boxes show a magnified view of three stimuli during one burst of the two BFS protocols. The same plasticity induction protocols were used in experiments in which MF inputs were activated by extracellular stimulation. (*C*) Representative individual PII recording in which posttetanic potentiation (PTP) and long-term potentiation (LTP) were induced by an aBFS applied at $t = 0$ ms (arrow). The amplitude of extracellularly evoked EPSCs is plotted against time. Each circle (○) denotes the peak amplitude of an individual EPSC recorded in an identified PII. LTP was measured 15–20 min after aBFS application (gray area). The group 2 mGluR agonist DCG-IV (0.5 μM) was bath-applied to confirm the MF-mediated nature of evoked EPSCs (gray area at 28–33 min of recording time). The horizontal black line indicates the time of agonist bath application. (*D*) LTP was readily evoked by an aBFS in PIIs when 0.1 mM spermine was added to the pipette solution, indicating that intracellular polyamines do not abolish Hebbian LTP induction (four PIIs). (*E*) Blockade of Ca^{2+}-permeable AMPA receptors (CP-AMPARs) with 50 μM 1-Naphthyl acetyl spermine trihydrochloride (NASPM) abolishes MF-LTP. Two independent MF inputs converging onto one target PII were stimulated extracellularly, and the baseline-normalized amplitudes of evoked EPSCs are plotted over time (five PIIs). NASPM was bath-applied, and an aBFS was applied to one of the two inputs (red ○), whereas the other one served as a control (gray ○). NASPM was washed out immediately after aBFS application. EPSCs of the input exposed to aBFS (red) showed marked PTP in contrast to the unstimulated one. However, both inputs were indistinguishable in peak amplitude 15–20 min after washout of NASPM, indicating the absence of LTP (see also ref. 8). (*F*) Bar graphs summarize the EPSC amplitudes evoked shortly after the aBFS application (PTP) and 15–20 min after the aBFS (LTP) for the stimulated input (red bars) in comparison to the nonstimulated input (gray bars). Gray circles (○) connected by lines represent data from individual experiments, and bars with lines indicate mean ± SEM.

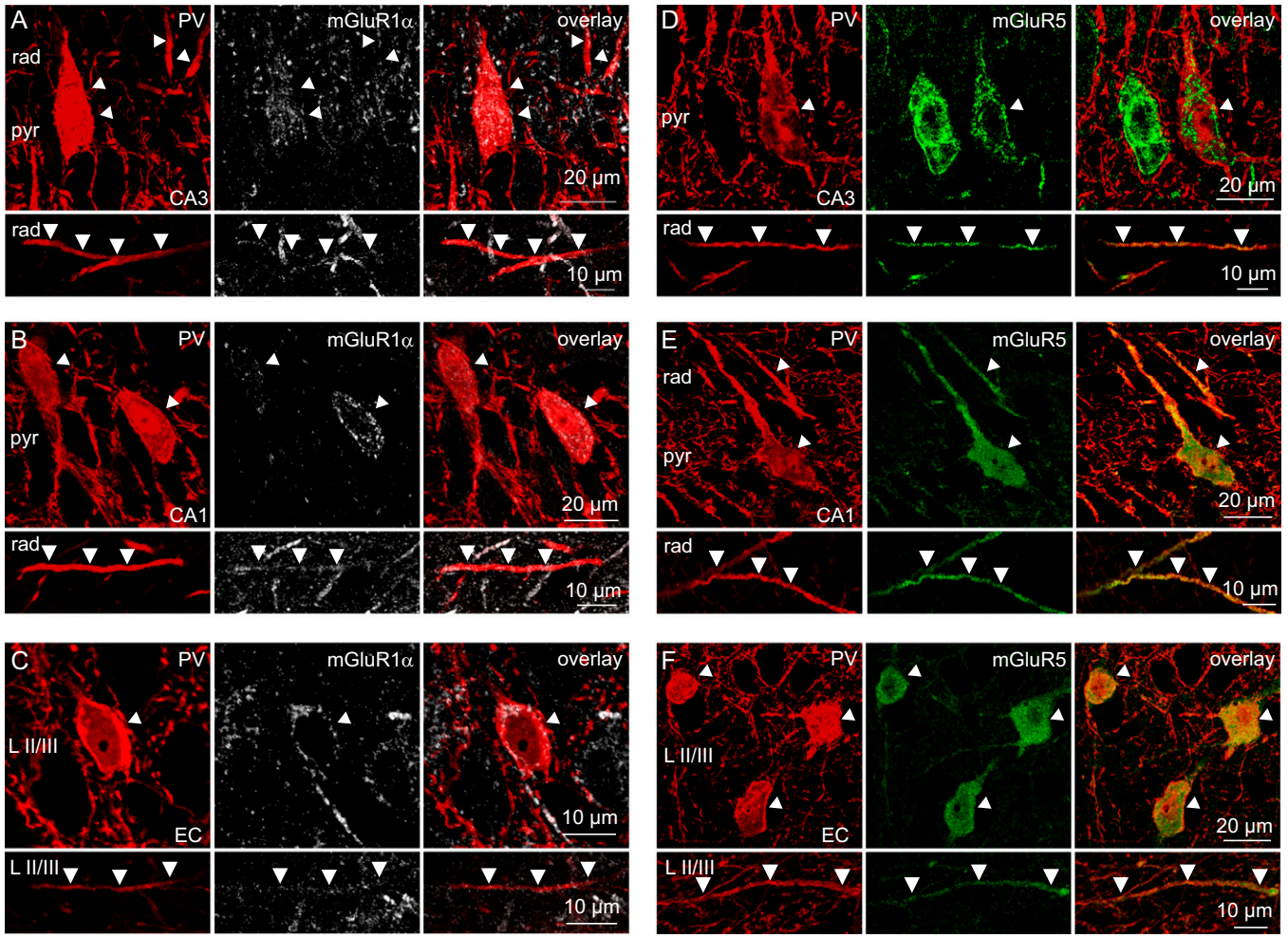

Fig. S2. Group I mGluRs are expressed in PV^+ interneurons throughout the hippocampus. (*Upper*) Immunolabeling against PV (red, *Left*), mGluR1α (white, *Center*), and overlay of both (*Right*) in the stratum pyramidale (pyr) of CA3 (*A*), CA1 (*B*), and layer II and III of the entorhinal cortex (EC) (*C*). (*Lower*) Images of PV^+ dendrites (arrowheads) from stratum radiatum (rad) (*A* and *B*) and from layer II/III (LII/III) (*C*). (*D–F*) Same as in *A–C*, but with immunolabeling against PV (red) and mGluR5 (green). Note that most intensive labeling for mGluR5 appeared in PV^+ cells. In contrast, labeling for mGluR1α was present in most PV^+ neurons, but it was considerably stronger in PV^- interneurons.

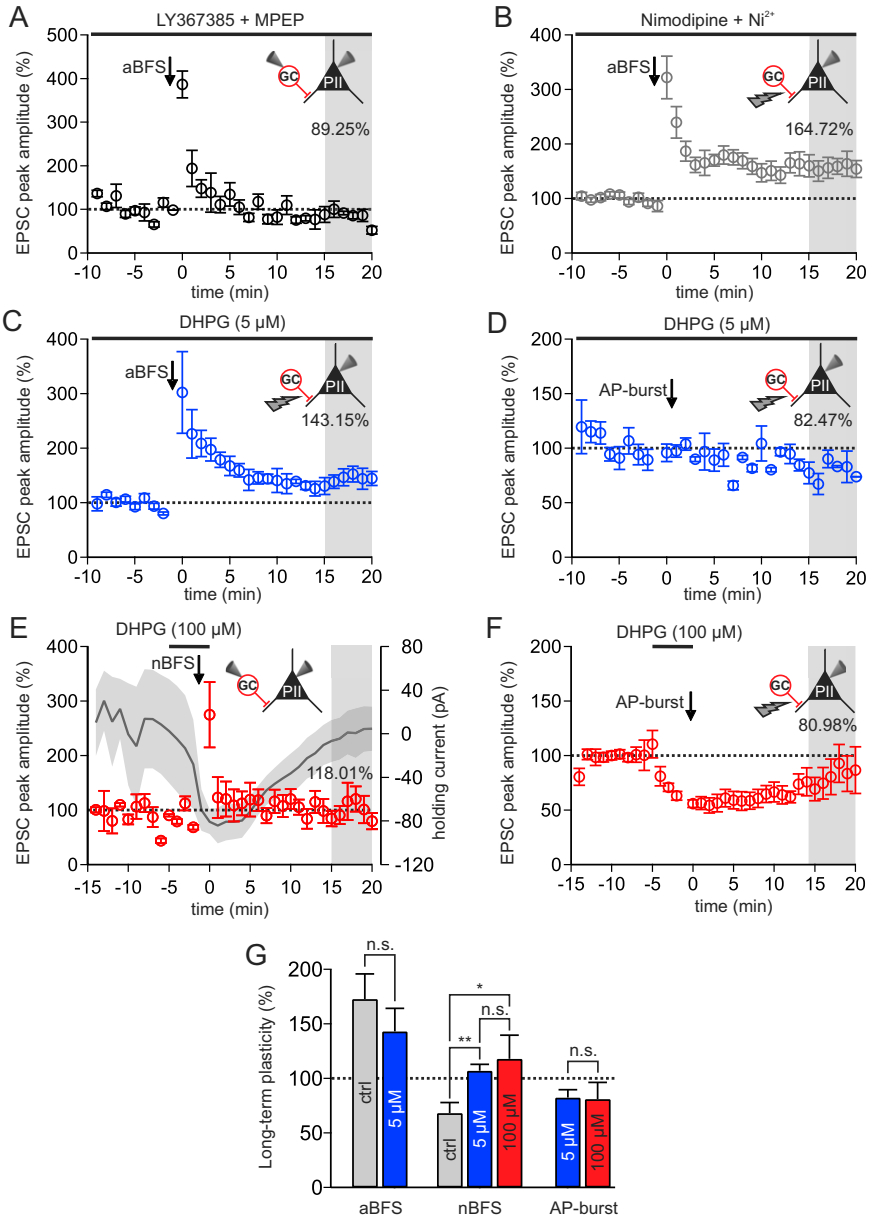

Fig. S3. Effects of pharmacological inhibition or activation of group I mGluRs on the expression of synaptic plasticity at MF-PII contacts. (*A–E*) Mean peak amplitudes of MF-mediated EPSCs were normalized to baseline values, binned minute-wise, and plotted against time. An aBFS, an nBFS, or bursts of APs (12 bursts, with each burst consisting of 25 APs at 30 Hz repeated at 0.33 Hz) were applied at $t = 0$ ms (arrows). Changes in synaptic efficacy were quantified 15–20 min after application of the protocols (gray area) and are indicated by the corresponding values. Horizontal lines show the time and duration of bath application of agonists and antagonists. (*A*) Plot summarizes the amplitude of normalized MF-mediated uEPSCs in the presence of LY367385 plus 2-Methyl-6-(phenylethynyl)pyridine hydrochloride (MPEP; four GC-PII pairs). Note Hebbian MF-LTP by aBFS are abolished when mGluR1α and mGluR5 are blocked. (*B*) LTP could still be elicited during blockade of VDCCs with nimodipine (10 µM) and Ni^{2+} (50 µM, five PIIs). (*C*) MF-LTP was not altered in the presence of the group I mGluR agonist DHPG (5 µM, four PIIs; $P = 0.975$ compared with control LTP). (*D*) Plot summarizes the amplitude of MF-mediated EPSCs before and after application of the AP protocol at $t = 0$ ms (arrow). Note that in the presence of DHPG, bursts of APs did not induce MF-LTP (four PIIs). (*E*) DHPG (100 µM) was briefly washed into the bath, and the nBFS protocol was applied immediately after the onset of the DHPG effect detected by a transient increase in the PII holding current (dark gray trace with gray shading indicates mean ± SEM). DHPG was washed out right after nBFS application (four pairs). Note that nBFS-induced long-term depression (LTD) was blocked by this procedure equally well as nBFS-induced LTD during the continuous presence of DHPG at low concentrations (5 µM) in the bath (Fig. 3*D*). These data indicate that brief activation of group I mGluRs during nBFS application is sufficient to inhibit LTD induction and excludes the possibility that constant activation of mGluRs occluded the expression of LTD, as shown in Fig. 3*D*. (*F*) Pairing postsynaptic AP bursts (arrow) with brief high-dose DHPG application did not induce LTP (six PIIs), indicating that even during strong group I mGluR activation and AP-mediated activation of VDCCs, CP-AMPAR–mediated synaptic Ca^{2+} signaling is still required for LTP induction. (*G*) Bar graph summarizing the effect of DHPG paired with an aBFS (*Left* group), nBFS (*Center* group), or postsynaptic AP bursts (*Right* group) protocol on the induction of MF-LTP. Bars represent the means from 25, 4, 10, 7, 4, 4, and 6 individual experiments (left to right). Blue bars represent data in which 5 µM DHPG was applied, and red bars represent data in which 100 µM DHPG was applied. Circles and bars with lines represent mean ± SEM. $*P \leq 0.05$; $**P \leq 0.01$; n.s., not significant ($P > 0.05$). GC, granule cell.

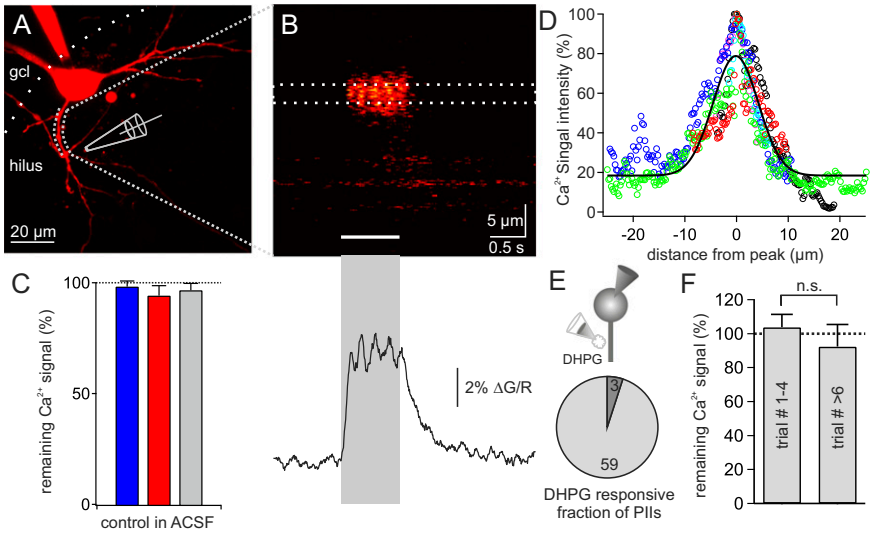

Fig. S4. MF-mediated Ca^{2+} signals in PIIs show narrow spatial localization and are stable over time. (*A*) Z-projection of a confocal image stack from a PII loaded with Alexa Fluor 594. Dotted lines indicate the trajectory of a longitudinal line scan through the basal PII dendrite close to the stimulation electrode (distance of ~10 µm). (*B*) Change of peak fluorescence (ΔG/R) along the scan line indicated in *A* evoked by a burst of extracellular MF stimulation (25 stimuli at 30 Hz; white bar represents duration of the stimulus). Note that the EPSC-mediated Ca^{2+} signal is confined sharply to a segment of ~5 µm, with little lateral spread from the putative postsynaptic location. The trace below the image shows the ΔG/R change in the dendritic area indicated by dotted lines. (*C*) Ca^{2+} signals evoked by APs (blue), MF-EPSCs (red), and one burst of an aBFS protocol (gray) are stable over the time course of our pharmacological experiments. Bars summarize the AP-mediated (blue), EPSC-mediated (red), and aBFS-mediated (gray) Ca^{2+} signals normalized to the initial measurement of the same signals performed 5–10 min earlier. All values are close to 100%, indicating stability of the Ca^{2+} measurements over time. Bars represent the average value ± SEM from 26 PIIs. (*D*) Lateral spread of synaptically evoked Ca^{2+} signals in basal PII dendrites. Peaks of the Ca^{2+} transients were measured along a longitudinal scan line following a basal PII dendrite as depicted in *A*. Peaks were aligned and normalized to the maximal Ca^{2+} elevation in the center of the synaptic hot spot. Data points were fit with a Gaussian function (black line). Colored circles (○) represent data points from individual experiments (six PIIs). (*E*) Pie chart illustrates the fraction of PIIs that showed a Ca^{2+} signal in response to DHPG puff application (59 of 62 PIIs). (*F*) Ca^{2+} transients elicited by DHPG puffs (20–100 ms, every 3 min) were stable over trials in a given PII under control conditions. (*Left* bar) Summary of the normalized Ca^{2+} response in the first to fourth trials (our control period; Fig. 4 *E*–*G*). (*Right* bar) Summary of the response from the sixth trial onward (the period in which we measured the effect of pharmacological manipulations; five PIIs). n.s., $P > 0.05$.

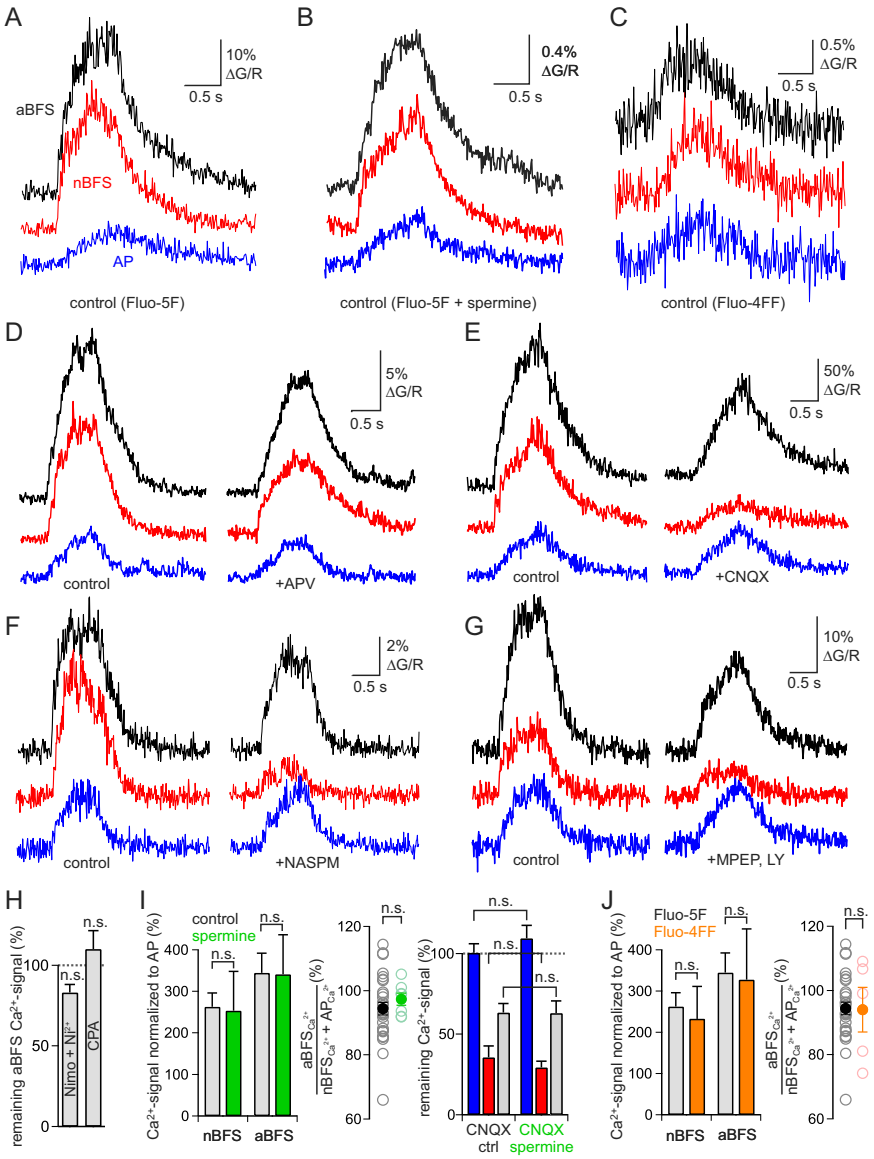

Fig. S5. Ca^{2+} signaling at MF-PII synapses under various pharmacological conditions is not affected by the blockade of CP-AMPARs by the polyamine analog spermine and does not saturate the Ca^{2+} indicator Fluo-5F. (*A*) Individual traces of aBFS-evoked (black), nBFS-evoked (red), and AP burst-evoked (blue) Ca^{2+} signals in PIIs measured with Fluo-5F under control conditions. All traces were filtered at 100 Hz. (*B*) Same as in *A*, but 0.1 mM spermine was added to the pipette solution. (*C*) Same as in *A*, but Ca^{2+} transients were measured with the low-affinity Ca^{2+} dye Fluo-4FF. (*D*) Ca^{2+} traces as in A, measured before (*Left*) and after (*Right*) the blockade of NMDA receptors (NMDARs) with 100 μM APV. (*E*) Ca^{2+} signals were measured similar to the ones shown in *D*, before (*Left*) and after (*Right*) AMPAR blockade with 20 μM 6-Cyano-7-nitroquinoxaline-2,3-dione (CNQX). (*F*) Same as in *E*, but CP-AMPARs were specifically blocked with 50 μM NASPM. (*G*) Ca^{2+} signals were measured as in *E*, before (*Left*) and after (*Right*) blockade of both group I mGluRs by coapplication of 10 μM MPEP and 100 μM LY367385 (LY). (*H*) Bar graphs summarize the effect of L-, R-, and T-type VDCC blockade by 10 μM nimodipine (Nimo) and 50 μM Ni^{2+} (*Left* bar, four PIIs) and depletion of intracellular Ca^{2+} stores with 30 μM CPA (*Right* bar, three PIIs) on aBFS-evoked Ca^{2+} transients. Note that the contribution of VDCCs to aBFS-induced Ca^{2+} signals is small and that both VDCCs and Ca^{2+} release from intracellular stores had no significant effect on Ca^{2+} signaling during aBFS application. (*I*, *Left*) Bar graph summarizes the nBFS-evoked (*Left* group) and aBFS-evoked (*Right* group) Ca^{2+} signals normalized to AP-evoked Ca^{2+} signals under control conditions (gray bars, 28 PIIs) and under conditions of PII loading with spermine (green bars, seven PIIs). Note that spermine had no effect on the amplitude of synaptically or aBFS-evoked Ca^{2+} signals. (*I*, *Center*) Linearity index of summation of nBFS- and AP-evoked Ca^{2+} signals with (green) and without (gray) spermine in the pipette solution. There was no significant effect of spermine on signal summation. (*I*, *Right*) Bar graph summarizes the reduction of AP-evoked (blue), nBFS-evoked (red), and aBFS-evoked (gray) Ca^{2+} signals by CNQX in control conditions (ctrl, 10 PIIs) and with spermine in the intracellular solution (five PIIs). The apparent contribution of AMPARs to the Ca^{2+} signals was not significantly different among groups. (*J*) Same as in *I* (*Left*), but the amplitude of Ca^{2+} signals obtained in controls using the Ca^{2+} indicator Fluo-5F was compared with recordings with the low-affinity Ca^{2+} indicator Fluo-4FF (five PIIs). No significant differences were observed between the two sets of measurements, indicating that Ca^{2+} signals were not saturating Fluo-5F. n.s., $P > 0.05$. Bars and circles with lines indicate mean ± SEM.